The Astrophysical Journal, 761:183 (9pp), 2012 December 20 doi:10.1088/0004-637X/761/2/183

HIGH-REDSHIFT COOL-CORE GALAXY CLUSTERS DETECTED VIA THE SUNYAEV–ZEL'DOVICH EFFECT IN THE SOUTH POLE TELESCOPE SURVEY

D. R. Semler[1], R. Šuhada[1], K. A. Aird[2], M. L. N. Ashby[3], M. Bautz[4], M. Bayliss[3,5], G. Bazin[1,6], S. Bocquet[1], B. A. Benson[7,10], L. E. Bleem[7,8], M. Brodwin[9], J. E. Carlstrom[7,8,10,11,12], C. L. Chang[7,10,12], H. M. Cho[13], A. Clocchiatti[14], T. M. Crawford[7,11], A. T. Crites[7,11], T. de Haan[15], S. Desai[1,6], M. A. Dobbs[15], J. P. Dudley[15], R. J. Foley[3], E. M. George[16], M. D. Gladders[7,11], A. H. Gonzalez[17], N. W. Halverson[18], N. L. Harrington[16], F. W. High[7,11], G. P. Holder[15], W. L. Holzapfel[16], S. Hoover[7,10], J. D. Hrubes[2], C. Jones[3], M. Joy[19], R. Keisler[7,8], L. Knox[20], A. T. Lee[16,21], E. M. Leitch[7,11], J. Liu[1,6], M. Lueker[16,22], D. Luong-Van[2], A. Mantz[7,11], D. P. Marrone[23], M. McDonald[4], J. J. McMahon[7,10,24], J. Mehl[7,11], S. S. Meyer[7,8,10,11], L. Mocanu[7,11], J. J. Mohr[1,6,25], T. E. Montroy[26], S. S. Murray[3], T. Natoli[7,8], S. Padin[7,11,22], T. Plagge[7,11], C. Pryke[27], C. L. Reichardt[16], A. Rest[28], J. Ruel[5], J. E. Ruhl[26], B. R. Saliwanchik[26], A. Saro[1], J. T. Sayre[26], K. K. Schaffer[7,10,29], L. Shaw[15,30], E. Shirokoff[16,22], J. Song[24], H. G. Spieler[21], B. Stalder[3], Z. Staniszewski[26], A. A. Stark[3], K. Story[7,8], C. W. Stubbs[3,5], A. van Engelen[15], K. Vanderlinde[15], J. D. Vieira[7,8,22], A. Vikhlinin[3], R. Williamson[7,11], O. Zahn[16,31], and A. Zenteno[1,6]

[1] Department of Physics, Ludwig-Maximilians-Universität, Scheinerstr. 1, D-81679 München, Germany
[2] University of Chicago, 5640 South Ellis Avenue, Chicago, IL 60637, USA
[3] Harvard-Smithsonian Center for Astrophysics, 60 Garden Street, Cambridge, MA 02138, USA
[4] MIT Kavli Institute for Astrophysics and Space Research, Massachusetts Institute of Technology, 77 Massachusetts Avenue, Cambridge, MA 02139, USA
[5] Department of Physics, Harvard University, 17 Oxford Street, Cambridge, MA 02138, USA
[6] Excellence Cluster Universe, Boltzmannstr. 2, D-85748 Garching, Germany
[7] Kavli Institute for Cosmological Physics, University of Chicago, 5640 South Ellis Avenue, Chicago, IL 60637, USA
[8] Department of Physics, University of Chicago, 5640 South Ellis Avenue, Chicago, IL 60637, USA
[9] Department of Physics and Astronomy, University of Missouri, 5110 Rockhill Road, Kansas City, MO 64110, USA
[10] Enrico Fermi Institute, University of Chicago, 5640 South Ellis Avenue, Chicago, IL 60637, USA
[11] Department of Astronomy and Astrophysics, University of Chicago, 5640 South Ellis Avenue, Chicago, IL 60637, USA
[12] Argonne National Laboratory, 9700 S. Cass Avenue, Argonne, IL 60439, USA
[13] NIST Quantum Devices Group, 325 Broadway Mailcode 817.03, Boulder, CO 80305, USA
[14] Departamento de Astronomía y Astrofísica, PUC Casilla 306, Santiago 22, Chile
[15] Department of Physics, McGill University, 3600 Rue University, Montreal, Quebec H3A 2T8, Canada
[16] Department of Physics, University of California, Berkeley, CA 94720, USA
[17] Department of Astronomy, University of Florida, Gainesville, FL 32611, USA
[18] Department of Astrophysical and Planetary Sciences and Department of Physics, University of Colorado, Boulder, CO 80309, USA
[19] Department of Space Science, VP62, NASA Marshall Space Flight Center, Huntsville, AL 35812, USA
[20] Department of Physics, University of California, One Shields Avenue, Davis, CA 95616, USA
[21] Physics Division, Lawrence Berkeley National Laboratory, Berkeley, CA 94720, USA
[22] California Institute of Technology, 1200 E. California Blvd., Pasadena, CA 91125, USA
[23] Steward Observatory, University of Arizona, 933 North Cherry Avenue, Tucson, AZ 85721, USA
[24] Department of Physics, University of Michigan, 450 Church Street, Ann Arbor, MI 48109, USA
[25] Max-Planck-Institut für extraterrestrische Physik, Giessenbachstr. D-85748 Garching, Germany
[26] Physics Department, Center for Education and Research in Cosmology and Astrophysics, Case Western Reserve University, Cleveland, OH 44106, USA
[27] Physics Department, University of Minnesota, 116 Church Street S.E., Minneapolis, MN 55455, USA
[28] Space Telescope Science Institute, 3700 San Martin Dr., Baltimore, MD 21218, USA
[29] Liberal Arts Department, School of the Art Institute of Chicago, 112 S Michigan Ave, Chicago, IL 60603, USA
[30] Department of Physics, Yale University, P.O. Box 208210, New Haven, CT 06520-8120, USA
[31] Berkeley Center for Cosmological Physics, Department of Physics, University of California, and Lawrence Berkeley National Labs, Berkeley, CA 94720, USA
Received 2012 August 16; accepted 2012 October 30; published 2012 December 6

ABSTRACT

We report the first investigation of cool-core properties of galaxy clusters selected via their Sunyaev–Zel'dovich (SZ) effect. We use 13 galaxy clusters uniformly selected from 178 deg^2 observed with the South Pole Telescope (SPT) and followed up by the *Chandra X-ray Observatory*. They form an approximately mass-limited sample ($>3 \times 10^{14}\ M_\odot\ h_{70}^{-1}$) spanning redshifts $0.3 < z < 1.1$. Using previously published X-ray-selected cluster samples, we compare two proxies of cool-core strength: surface brightness concentration ($c_{\rm SB}$) and cuspiness (α). We find that $c_{\rm SB}$ is better constrained. We measure $c_{\rm SB}$ for the SPT sample and find several new $z > 0.5$ cool-core clusters, including two strong cool cores. This rules out the hypothesis that there are no $z > 0.5$ clusters that qualify as strong cool cores at the 5.4σ level. The fraction of strong cool-core clusters in the SPT sample in this redshift regime is between 7% and 56% (95% confidence). Although the SPT selection function is significantly different from the X-ray samples, the high-z $c_{\rm SB}$ distribution for the SPT sample is statistically consistent with that of X-ray-selected samples at both low and high redshifts. The cool-core strength is inversely correlated with the offset between the brightest cluster galaxy and the X-ray centroid, providing evidence that the dynamical state affects the cool-core strength of the cluster. Larger SZ-selected samples will be crucial in understanding the evolution of cluster cool cores over cosmic time.

Key words: galaxies: clusters: general – X-rays: galaxies: clusters

Online-only material: color figures

1. INTRODUCTION

Galaxy clusters grow over cosmic time through mergers with other galaxy clusters as well as through the accretion of gas and individual galaxies from the surrounding environment. On timescales of a few Gyr, radiative cooling due to X-ray emission from the intracluster medium (ICM) would give rise to a "cooling flow" to the cluster core (Fabian & Nulsen 1977; Mathews & Bregman 1978), if it were not countered by a heating mechanism. These cooling flows are not observed; instead, the cores of some clusters are found to undergo only moderate cooling (Kaastra et al. 2001; Peterson et al. 2001; Tamura et al. 2001). Such galaxy clusters are known as "cool-core" clusters (Molendi & Pizzolato 2001). Other clusters exhibit little to no cooling in their core (i.e., noncool-core clusters). These cooling properties suggest that there must be processes in every cluster that are strong enough to either regulate cooling flows or completely prevent them. Such processes are not fully understood and it is still uncertain how they evolve and affect cluster formation over time.

The important astrophysical processes that counteract cool-core formation are typically thought to fall under three broad categories: feedback from active galactic nuclei (AGNs), preheating of the cluster gas, and cluster mergers. AGN feedback in the cluster's brightest cluster galaxy (BCG) has been shown to be capable of regulating cooling flows in cool-core clusters (see Fabian 2012; McNamara & Nulsen 2012, for reviews). In some cases, the feedback may be strong enough to disrupt a cool core completely (e.g., McDonald et al. 2011), though this phenomenon is likely limited to lower mass galaxy clusters and groups. Additionally, AGN feedback may drive turbulence in the ICM. This has been shown to suppress heat-flux-driven buoyancy instabilities, resulting in effective transfer of heat from the outer radii and disrupting the cool core (Parrish et al. 2012). Heating of the intracluster gas during early stages of the cluster has been shown to affect the formation of cool cores as well (e.g., Kaiser 1991; McCarthy et al. 2008; Sun 2009). Cluster mergers can also disrupt cool cores by shock-heating and turbulent mixing, a process that has been reproduced in simulations (e.g., McGlynn & Fabian 1984; Gómez et al. 2002; ZuHone et al. 2010). Whether a merger can destroy a cool core likely depends on the strength of the cool core, the mass ratio of the merging clusters, and the geometry of the impact.

Studying the evolution of clusters can provide insight regarding the relative importance of these processes in cool-core formation. Given that cool cores develop over a central cooling time of typically a few Gyr, one expects there to be fewer cool cores at times closer to the epoch of galaxy cluster formation. Simulations predict a significantly higher cluster merger rate in the past (Gottlöber et al. 2001). If mergers play a strong role in the disruption of cool-core galaxy clusters, this too suggests that the fraction of galaxy clusters with cool cores should be lower at high redshifts than in local samples. Indeed, studies of the evolution of the cool-core fraction find a much lower fraction at $z = 0.5$ (McDonald 2011) and a significant dearth in *strong* cool cores at $z > 0.5$ (Vikhlinin et al. 2007; Santos et al. 2010; Samuele et al. 2011). To date, only a small number of $z > 0.5$ galaxy clusters with possible strong cool cores have been reported (e.g., Siemiginowska et al. 2010; Russell et al. 2012), with the most dramatic, confirmed strong cool core coming from the South Pole Telescope (SPT) survey (McDonald et al. 2012).

Understanding cool-core evolution is complicated by selection biases of cluster samples. One can generically expect an X-ray-selected sample to be biased toward selecting cool-core galaxy clusters (Hudson et al. 2010; Eckert et al. 2011) due to their higher X-ray surface brightness and luminosity as compared with a noncool-core galaxy cluster of the same mass (e.g., O'Hara et al. 2006). However, there are competing effects due to X-ray emission from AGNs, which are expected to be more prevalent at higher redshifts (Russell et al. 2012). The bias may be complicated further by the ways in which different cluster-finding algorithms differentiate between point sources (e.g., AGNs, X-ray binaries) and extended sources (e.g., nearby galaxies, groups, and clusters). Furthermore, the classification of the cool-core strength of a cluster varies between surveys of different angular resolution and the method used to characterize the cool core.

Given the complex effects associated with X-ray selection, it is important to investigate the cool-core fraction and its evolution using an independent selection method. In this paper, we study the cool-core properties of galaxy clusters selected from their Sunyaev–Zel'dovich (SZ) effect (Sunyaev & Zel'dovich 1972) signature in the SPT survey. At $z > 0.3$, this SPT selection is nearly redshift-independent and nearly constant in mass (e.g., Reichardt et al. 2012). The SZ effect selection is expected to be relatively insensitive to non-gravitational physics (Nagai 2006), the dynamical state of clusters (Jeltema et al. 2008), radio contamination from point sources and BCGs (Lin et al. 2009), and the presence of cool cores (Motl et al. 2005). Therefore, an SZ-cluster survey is expected to be a useful tool to study the redshift evolution of galaxy cluster properties. This work provides the first glimpse of the cool-core properties of a sample of galaxy clusters selected from the SZ effect.

The layout of this paper is as follows. In Section 2, we detail the observations used and describe the data reduction procedures. In Section 3, we present the steps used to make our measurements as well as compare two methods used to characterize cool-core strengths that are suitable for high-redshift clusters. In Section 4, we present the results of our measurements and investigate the implications for the cool-core fraction at high redshifts. In Section 5, we investigate the relationship between a cluster's cool-core strength and the offset of its BCG. Finally, in Section 6, we conclude our analyses and present future studies and applications.

In this analysis, we assume the best-fit WMAP7+BAO+H_0 flat ΛCDM cosmology (Komatsu et al. 2011) with Hubble parameter $H_0 = 70.4$ km s^{-1} Mpc^{-1}, matter density $\Omega_M = 0.272$, and dark energy density $\Omega_\Lambda = 0.728$.

2. OBSERVATIONS

We analyze *Chandra* data for two different cluster samples, an SZ-selected sample from Andersson et al. (2011, hereafter A11) and an X-ray-selected sample from Vikhlinin et al. (2009, hereafter V09). In this section, we describe each cluster sample and the *Chandra* X-ray data reduction.

2.1. Cluster Samples

We first describe the SZ-selected sample from A11. This cluster sample is a subset of the SPT cluster catalog described by Vanderlinde et al. (2010), which consists of 21 clusters selected by their SZ-significance (ξ) from 178 deg^2 of sky surveyed by the SPT. From the subsample of 17 clusters at $z > 0.3$ and $\xi > 5.45$, 15 clusters were selected for X-ray observations, the

results of which are discussed in A11 and Benson et al. (2011). Of the 15 observations, 13 were carried out by *Chandra* and two were carried out by *XMM-Newton*. For this study, we use the 13 clusters with *Chandra* observations because only *Chandra* provides the spatial resolution needed for our analysis. These 13 clusters form a *nearly* complete mass-limited sample (called the "SPT sample").

In addition to these, we analyze SPT-CL J2106−5844, a massive galaxy cluster at $z = 1.13$ discovered by the SPT survey (Foley et al. 2011). However, this cluster is not included in analyses involving the distribution of cool-core strengths (Section 4.3) as it is not a member of the mass-limited data set.

We also analyze 41 galaxy clusters, based largely from the high-redshift sample of the Chandra Cluster Cosmology Project,[32] known hereafter as the CCCP high-z sample (V09). This X-ray-selected sample is the subset of clusters in the 400d survey (Burenin et al. 2007) at $z \geqslant 0.35$ and above a redshift-dependent X-ray-luminosity threshold. We include five additional clusters from the 400d survey with *Chandra* data available not presented in V09.[33]

2.2. Chandra Data Reduction

The *Chandra* observations used in this study are listed in Table 1. Data are reduced using the *Chandra* software version `CIAO 4.4` and `CALDB 4.4.8`. For all observations, Level = 2 event files are generated with the `chandra_repro` script. Exposure corrections are applied using `fluximage` in the 0.5–2 keV band with exposure maps calculated at 1.5 keV. We employ a two-step procedure in removing point sources. First, candidate point sources are identified using `wavdetect`. The results are then visually inspected and false detections within the cluster are ignored. Using `dmfilth`, proper detections are replaced with a level determined from an elliptical annulus centered on the point source. Background levels are determined in each observation from several regions located on the same chip as the cluster source without point source detections. The regions are positioned far enough from the cluster emission so as to contain negligible cluster photons and are large enough to adequately sample the background level.

The results enable measurements to be made on the background-subtracted, exposure-corrected, flux images in the 0.5–2 keV band where each pixel is in units of photons $\mathrm{cm}^{-2}\ \mathrm{s}^{-1}$. Count-rate errors are determined based on Poisson statistics and propagated in the standard way.

3. MEASURING COOL CORES WITH IMAGING DATA

Hudson et al. (2010) compare several X-ray estimators of cool-core strength that are applied to a cluster sample with a range of X-ray data quality and redshifts. They find that the X-ray cuspiness (α; Vikhlinin et al. 2007) and the surface brightness concentration (c_{SB}; Santos et al. 2008) are promising cool-core estimators for high-redshift clusters with observations containing relatively few X-ray photons. In the low-redshift regime, they find the central cooling time, t_{cool} to be the best cool-core estimator based on the strength of its bimodality. Both c_{SB} and α have been shown to correlate well with the central cooling time (Santos et al. 2008; Hudson et al. 2010). In this section, we compare the α and c_{SB} parameters to the central cooling time for a wider sample of clusters. We also calculate c_{SB} for the portion of the CCCP high-z sample not previously published (i.e., clusters at $z < 0.5$).

Table 1
Chandra Observation IDs

Cluster	Observation ID
SPT-CL J0000–5748	9335
SPT-CL J0509–5342	9432
SPT-CL J0516–5430	9331
SPT-CL J0528–5300	12092, 10862, 11996, 9341, 11874
SPT-CL J0533–5005	11748, 12001
SPT-CL J0546–5345	9336, 9332, 10864, 10851
SPT-CL J0551–5709	11871
SPT-CL J2106–5844	12180
SPT-CL J2331–5051	11738, 9333
SPT-CL J2337–5942	11859
SPT-CL J2341–5119	11799, 9345
SPT-CL J2342–5411	11870, 11741, 12014
SPT-CL J2355–5056	11998, 11746
SPT-CL J2359–5009	9334, 11742, 11864
CL J0340–2823	5780
CL J0302–0423	5782
CL J1212+2733	5767
CL J0350–3801	7227
CL J0318–0302	5775
CL J1514+3636	800
CL J0159+0030	5777
CL J0958+4702	5779
CL J0809+2811	5774
CL J1416+4446	541
CL J1312+3900	5781
CL J1003+3253	5776
CL J0141–3034	5778
CL J1701+6414	547
CL J1641+4001	3575
CL J0522–3624	4926, 5837
CL J1222+2709	5766
CL J0355–3741	5761
CL J0853+5759	4925, 5765
CL J0333–2456	5764
CL J0926+1242	4929, 5838
CL J0030+2618	5762
CL J1002+6858	5773
CL J1524+0957	1664
CL J1357+6232	5763, 7267
CL J1354–0221	4932, 5835
CL J1117+1744	4933, 5836
CL J1120+2326	3235
CL J0216–1747	5760, 6393
CL J0521–2530	5758
CL J0956+4107	5294, 5759
CL J0328–2140	5755, 6258
CL J1120+4318	5771
CL J1334+5031	5772
CL J0542–4100	914
CL J1202+5751	5757
CL J0405–4100	7191
CL J1221+4918	1662
CL J0230+1836	5754
CL J0152–1358	913
CL J1226+3332	3180, 5014

3.1. Calculating α and c_{SB}

The cuspiness is defined as the slope of the gas density ρ_g

$$\alpha \equiv -\frac{d \log \rho_g}{d \log r},$$

[32] http://hea-www.harvard.edu/400d/cosm/

[33] These clusters are included to increase the sample size as well as to remain consistent with the data set presented in Santos et al. (2010).

where the function is evaluated at radius $r = 0.04r_{500}$, r_{500} being the radius at which the mean density of the enclosed mass is 500 times that of the critical density at the object's redshift (Vikhlinin et al. 2007). This radius is close enough to the cluster core to sample the areas of strongest cooling, while still being far enough to avoid any flattening of the density profile caused by feedback from a central AGN. Calculations of α for the CCCP high-z sample are derived from the X-ray surface brightness fits and X-ray centers used in V09.

The $c_{\rm SB}$ is defined as the ratio of the soft X-ray flux, F, within the inner 40 kpc to the inner 400 kpc

$$c_{\rm SB} \equiv \frac{F_{r<40\,\rm kpc}}{F_{r<400\,\rm kpc}}$$

(Santos et al. 2008). These radii were chosen because they provide the largest separation of $c_{\rm SB}$ values between cool-core and noncool-core clusters. Previous studies have used either the 0.5–5.0 keV energy band or the 0.5–2.0 keV energy band for determining $c_{\rm SB}$. We follow Santos et al. (2010) in using the 0.5–2.0 keV band for our $c_{\rm SB}$ measurements.

To calculate $c_{\rm SB}$ in the clusters described in Section 2.1, we first estimate the centroid of the X-ray emission for each galaxy cluster. This is determined by iterating the centroid within an 80 pixel ($\sim$40″) radius, initially centered on the approximate location of the centroid. For each iteration, the centroid is calculated with the image weighted by $r^{-1/2}$, where r is radial distance to the center of the previous iteration. For clusters with multiple observations, an inverse variance weighted final $c_{\rm SB}$ is determined using the $c_{\rm SB}$ values measured in the individual observations. In these clusters, the X-ray centroid is taken to be the mean centroid of all observations, without any weighting applied.

When comparing X-ray measurements across different redshift regimes, a K-correction is commonly applied to account for the redshift dependence of the flux in a given band. This is generally a small effect for the $c_{\rm SB}$ parameter (Santos et al. 2010). We assume it's negligible for this work because we are primarily interested in comparing several galaxy cluster samples at similarly high redshifts.

Using the above analysis, we report α and $c_{\rm SB}$ for the CCCP high-z sample in Table 2, with $c_{\rm SB}$ values for clusters at $z \geqslant 0.5$ from Santos et al. (2010).

In the following analyses, we adopt the three different cool-core regimes defined previously for these parameters (Vikhlinin et al. 2007; Santos et al. 2008): the noncool-core regime ($c_{\rm SB} < 0.075$; $\alpha < 0.5$), the moderate regime ($0.075 < c_{\rm SB} < 0.155$; $0.5 < \alpha < 0.7$), and the strong cool-core regime ($c_{\rm SB} > 0.155$; $\alpha > 0.7$).

3.2. Comparison of $c_{\rm SB}$ and α

We study the performances of α and $c_{\rm SB}$ by first relating the two parameters to $t_{\rm cool}$ in a sample of low-redshift galaxy clusters. In Figure 1, we compare the measurements of $c_{\rm SB}$ and $t_{\rm cool}$ from Santos et al. (2008) with those of α and $t_{\rm cool}$ from Hudson et al. (2010). We note that Santos et al. (2008) calculate $c_{\rm SB}$ in a different band of 0.5–5.0 keV, however this should not qualitatively change our conclusions because the bulk of ICM emission is in the 0.5–2.0 keV band. We find α and $t_{\rm cool}$ to have a Spearman's rank correlation coefficient of $\rho_\alpha = -0.88$. The associated p-value corresponds to a probability of 4.4×10^{-22} that there is no correlation between the two parameters. The results are similar for $c_{\rm SB}$ and $t_{\rm cool}$; their Spearman's rank correlation coefficient is $\rho_{c_{\rm SB}} = -0.84$ with a p-value of 6.3×10^{-8}.

We compare the two parameters directly for the galaxy clusters in the CCCP high-z set. As shown in Figure 2, the α parameter exhibits larger fractional errors than $c_{\rm SB}$ in the CCCP high-z sample. This is particularly prevalent for low α, indicating that the parameter is less constrained in the noncool-core regime. Even excluding the six clusters where the signal-to-noise ratio (S/N) is less than 0.5, the median S/N in α is 2.9. However, for all clusters in this sample, the median S/N in $c_{\rm SB}$ is 7.8.

As shown in Figure 2, the two parameters do not always provide the same classification for a cluster's cool-core strength. The classification thresholds for $c_{\rm SB}$ and α were defined in Santos et al. (2008) and Vikhlinin et al. (2007), respectively. The definitions were based on separate data sets using

Table 2
CCCP High-z Galaxy Cluster Measurements

Cluster	z (1)	$c_{\rm SB}$	α
CL J0340−2823[a]	0.35	0.114 ± 0.012	0.920 ± 0.068
CL J0302−0423	0.35	0.374 ± 0.024	1.349 ± 0.053
CL J1212+2733	0.35	0.036 ± 0.005	0.389 ± 0.133
CL J0350−3801	0.36	0.073 ± 0.012	0.126 ± 0.176
CL J0318−0302	0.37	0.039 ± 0.007	0.078 ± 0.102
CL J1514+3636[a]	0.37	0.276 ± 0.014	1.185 ± 0.049
CL J0159+0030	0.39	0.175 ± 0.017	1.102 ± 0.071
CL J0958+4702	0.39	0.144 ± 0.016	0.751 ± 0.148
CL J0809+2811	0.40	0.028 ± 0.006	0.021 ± 0.089
CL J1416+4446	0.40	0.149 ± 0.012	1.008 ± 0.064
CL J1312+3900	0.40	0.046 ± 0.009	0.026 ± 0.036
CL J1003+3253	0.42	0.216 ± 0.022	1.369 ± 0.188
CL J0141−3034	0.44	0.058 ± 0.014	0.563 ± 0.284
CL J1701+6414	0.45	0.155 ± 0.013	1.189 ± 0.043
CL J1641+4001	0.46	0.087 ± 0.011	0.695 ± 0.314
CL J0522−3624	0.47	0.048 ± 0.008	0.671 ± 0.102
CL J1222+2709	0.47	0.115 ± 0.014	0.743 ± 0.132
CL J0355−3741	0.47	0.096 ± 0.013	0.877 ± 0.076
CL J0853+5759	0.48	0.025 ± 0.007	0.190 ± 0.208
CL J0333−2456	0.48	0.035 ± 0.007	0.395 ± 0.173
CL J0926+1242	0.49	0.092 ± 0.010	0.744 ± 0.116
CL J0030+2618	0.50	0.040 ± 0.011[b]	0.358 ± 0.155
CL J1002+6858	0.50	0.060 ± 0.012[b]	0.185 ± 0.147
CL J1524+0957	0.52	0.032 ± 0.006[b]	0.056 ± 0.698
CL J1357+6232	0.53	0.054 ± 0.010[b]	0.632 ± 0.113
CL J1354−0221	0.55	0.043 ± 0.009[b]	0.035 ± 0.434
CL J1117+1744[a]	0.55	0.041 ± 0.010[b]	0.322 ± 0.221
CL J1120+2326	0.56	0.027 ± 0.011[b]	0.280 ± 0.127
CL J0216−1747[a]	0.58	0.055 ± 0.014[b]	0.428 ± 0.203
CL J0521−2530[a]	0.58	0.046 ± 0.007[b]	0.500 ± 0.225
CL J0956+4107	0.59	0.040 ± 0.007[b]	0.026 ± 0.007
CL J0328−2140	0.59	0.062 ± 0.009[b]	0.513 ± 0.185
CL J1120+4318	0.60	0.063 ± 0.005[b]	0.679 ± 0.101
CL J1334+5031	0.62	0.068 ± 0.017[b]	0.381 ± 0.228
CL J0542−4100	0.64	0.043 ± 0.007[b]	0.454 ± 0.136
CL J1202+5751	0.68	0.030 ± 0.008[b]	0.009 ± 0.121
CL J0405−4100	0.69	0.073 ± 0.009[b]	0.293 ± 0.111
CL J1221+4918	0.70	0.026 ± 0.006[b]	0.049 ± 0.032
CL J0230+1836	0.80	0.036 ± 0.009[b]	0.161 ± 1.171
CL J0152−1358	0.83	0.027 ± 0.008[b]	0.102 ± 0.364
CL J1226+3332	0.89	0.086 ± 0.007[b]	0.333 ± 0.075

Notes. (1) Redshifts from Vikhlinin et al. (2009).
[a] Cluster not a member of the original CCCP high-z set presented in V09.
[b] $c_{\rm SB}$ values from Santos et al. (2010).

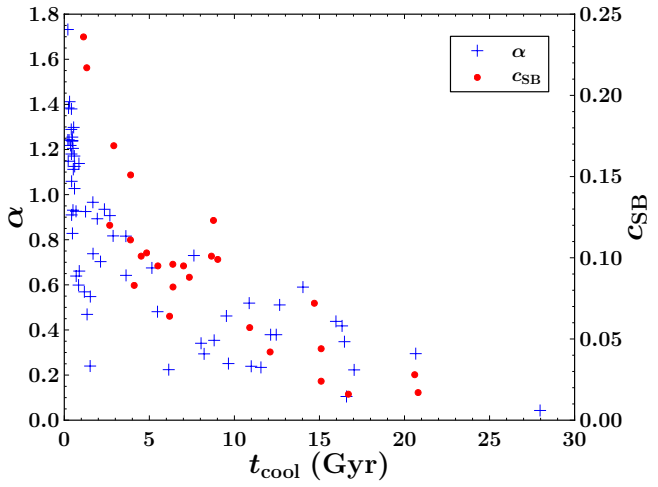

Figure 1. Comparison of α and c_{SB} with t_{cool}. Galaxy clusters with α and t_{cool} values are taken from Hudson et al. (2010) and galaxy clusters with c_{SB} and t_{cool} values are taken from Santos et al. (2008).

(A color version of this figure is available in the online journal.)

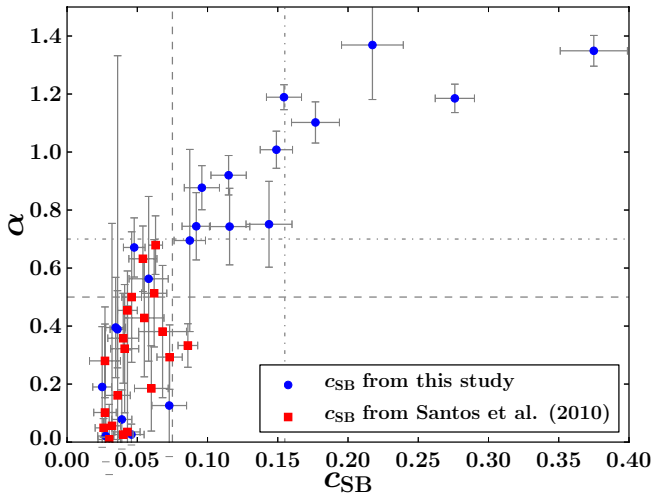

Figure 2. Correlation between α and c_{SB} for the CCCP high-z clusters. Values for α are from Vikhlinin et al. (2007). Values for c_{SB} with $z < 0.5$ are reported in this study. Values for c_{SB} with $z \geqslant 0.5$ are from Santos et al. (2010). The dashed lines correspond to the boundaries between noncool cores and moderate cool cores. The dash-dotted lines correspond to the boundaries between moderate cool cores and strong cool cores.

(A color version of this figure is available in the online journal.)

characteristics of each parameters' distribution. Therefore, one would not necessarily expect perfect agreement between the two parameters. Regardless, using these classifications, all strong cool-core clusters identified by c_{SB} are also classified as such when using α. Therefore, the c_{SB} parameter provides a more conservative threshold for identifying strong cool-core clusters.

Throughout the rest of the paper, we will use the c_{SB} parameter to characterize the cool-core strength of both the X-ray and SZ-selected samples. The X-ray observations of these samples have comparable S/N to the samples used in this section. Therefore, we expect similar performances from α and c_{SB} as was shown here, where the results suggest that c_{SB} is a more robust and comparably accurate cool-core proxy.

4. EVOLUTION OF THE COOL-CORE FRACTION

In this section, we compare the c_{SB} distribution as a proxy for the cool-core fraction for various comparable cluster samples. We first describe the X-ray-selected cluster samples previously studied and then go on to present the results for the SPT sample. We compare the c_{SB} distribution of the X-ray-selected sample with that of the SPT sample in different redshift regimes. Finally, we discuss systematics that could affect the SPT sample.

4.1. X-ray-selected Cluster Samples

Previously, Santos et al. (2010) compared the surface brightness concentrations for 57 galaxy clusters. They compared both low- and high-redshift samples as well as clusters selected by different X-ray selection methods. All of the clusters were first detected in *ROSAT* PSPC observations and were later followed up with *Chandra*. About half of the clusters (26) are from the $0.05 \leqslant z \leqslant 0.22$ portion of the CCCP low-z set (V09), a flux-limited cluster sample with many of the same members presented in Edge et al. (1990). The other half is comprised of clusters in the CCCP high-z set (V09) with $z \geqslant 0.5$ (20 clusters)[34] and the $z \geqslant 0.6$ clusters from the RDCS[35] (Rosati et al. 1998) and the WARPS[36] (Horner et al. 2008) samples that have *Chandra* observations (15 Clusters). One of these clusters, WARP J1415.1+3612, has an updated c_{SB} in Santos et al. (2012). Due to the low number of counts and similar selection properties in the RDCS and WARPS surveys, Santos et al. (2010) group them together in their analysis as RDCS+WARPS. For consistency, we follow the same practice here. Note that four clusters are members of both RDCS+WARPS and the CCCP high-z samples. There is one additional high-redshift cluster that has a published c_{SB} value, XMMU J1230.3+1339 (Fassbender et al. 2011).

Santos et al. (2010) compare the c_{SB} distributions of the CCCP high-z and RDCS+WARPS samples using a K-S test. The result yields a probability of only 0.6% for the null hypothesis that the two distributions are drawn from the same parent distribution. Santos et al. (2010) argue this is due to a bias of the detection algorithm used in CCCP against compact clusters with a relatively high mean surface brightness. This conflicts with Burenin et al. (2007), who tested the CCCP selection algorithm on a morphologically diverse set of cluster images, reprojected to redshifts between 0.35 and 0.80. The results showed comparable selection efficiencies for all of the cluster morphologies, indicating the selection method does not present a bias with respect to the cool-core strength of the cluster.

4.2. The SPT Sample

The SPT sample is described in Section 2.1. It consists of 13 clusters with X-ray observations that have been previously described in A11 and Benson et al. (2011). We also provide a c_{SB} measurement for SPT-CL J2106−5844, whose other X-ray properties are discussed in Foley et al. (2011). Their c_{SB} values are provided in Table 3.

In the SPT sample, we find two high-redshift galaxy clusters with surface brightness concentrations in the strong cool-core regime. These are among the first strong cool-core galaxy

[34] The 20 clusters from the CCCP high-z sample with $z \geqslant 0.5$ presented in Santos et al. (2010) include three clusters not in the original CCCP high-z sample, as their *Chandra* observations revealed they did not meet the flux criterion for membership.

[35] *ROSAT* Deep Cluster Survey.

[36] Wide Angle *ROSAT* Pointed Survey, http://asd.gsfc.nasa.gov/Donald.Horner/warps/index.html

Table 3
SPT Galaxy Cluster Measurements

Cluster	R.A. (1)	Decl. (1)	c_{SB}	z (2)	BCG Offset (3) (kpc)
SPT-CL J0000−5748	0.250	−57.810	0.244 ± 0.023	0.70	7.4 ± 3.5
SPT-CL J0509−5342	77.338	−53.703	0.109 ± 0.010	0.46	24.1 ± 2.9
SPT-CL J0516−5430	79.148	−54.506	0.026 ± 0.005	0.30	107.3 ± 2.2
SPT-CL J0528−5300	82.020	−52.997	0.061 ± 0.009	0.77	58.1 ± 3.7
SPT-CL J0533−5005	83.405	−50.098	0.013 ± 0.007	0.88	414.2 ± 3.8
SPT-CL J0546−5345	86.655	−53.759	0.072 ± 0.010	1.07	40.8 ± 4.0
SPT-CL J0551−5709	87.893	−57.144	0.034 ± 0.008	0.42	82.0 ± 2.7
SPT-CL J2106−5844[a]	316.518	−58.742	0.027 ± 0.007	1.13	24.3 ± 4.1
SPT-CL J2331−5051	352.963	−50.865	0.214 ± 0.016	0.58	4.5 ± 3.2
SPT-CL J2337−5942	354.353	−59.705	0.033 ± 0.006	0.78	199.4 ± 3.7
SPT-CL J2341−5119	355.301	−51.329	0.092 ± 0.009	1.00	3.0 ± 4.0
SPT-CL J2342−5411	355.692	−54.185	0.138 ± 0.013	1.08	8.6 ± 4.1
SPT-CL J2355−5056	358.948	−50.928	0.113 ± 0.010	0.32	6.7 ± 2.3
SPT-CL J2359−5009	359.931	−50.170	0.035 ± 0.007	0.78	85.5 ± 3.7

Notes. (1) Coordinates determined from X-ray centroid. (2) Redshifts from Song et al. (2012). (3) Projected offset between BCG position and X-ray centroid, with BCG positions taken from Song et al. (2012). The error in offset corresponds to the resolution limit of *Chandra* at the cluster's redshift.
[a] SPT-CL J2106−5844 is not included in the analysis of the c_{SB} distribution.

clusters detected at redshifts beyond $z = 0.5$. One of the strong cool-core clusters is SPT-CL J2331−5051, which lies at $z = 0.58$ and has a c_{SB} of 0.214 ± 0.016. The strongest cool-core cluster is SPT-CL J0000−5748 and has a c_{SB} of 0.244 ± 0.023. At a redshift of 0.702, corresponding to 7.4 Gyr after the big bang, this cluster is also the highest redshift strong cool-core cluster found in this work. These two clusters rule out the hypothesis that there are no galaxy clusters at $z > 0.5$ classified by c_{SB} as having strong cool cores at the 5.4σ level.

The X-ray properties of the galaxy cluster SPT-CL J2106−5844 were studied in detail in Foley et al. (2011). With a mass $M_{200} = (1.27 \pm 0.21) \times 10^{15}\, h_{70}^{-1}\, M_{\odot}$ and a redshift $z = 1.13$, it is the most massive cluster known at $z > 1$. They measure a cluster temperature of $T_X = 11.0^{+2.6}_{-1.9}$ keV and a central temperature of $T_X = 6.5^{+1.7}_{-1.1}$ keV within $0.17 r_{500}$. The temperature decrement in the core suggests moderate cooling. We measure the surface brightness concentration $c_{SB} = 0.026 \pm 0.007$, which lies below the moderate cool-core threshold.

4.3. c_{SB} Distribution

In this section, we compare the c_{SB} distributions of the SPT and X-ray-selected high-redshift cluster samples. To remain consistent with Vikhlinin et al. (2007) and Santos et al. (2010), we define a redshift break in our cluster samples at $z = 0.5$, with clusters at $z \geqslant 0.5$ defined to be "high-z" and clusters at $z < 0.5$ defined to be "low-z." We do not include SPT-CL J2106−5844 in these analyses as it is not part of a uniformly SZ-selected sample with X-ray follow-up, as is approximately the case for the clusters studied in A11.

The distribution of c_{SB} as a function of redshift for various X-ray-selected samples and the SPT sample is in Figure 3. At $z > 0.5$, there are 31 clusters in X-ray-selected samples and nine in the SPT sample. In this regime, there are only two strong cool-core clusters, both in the SPT sample. This constrains the fraction of strong cool cores at high redshifts in the SPT sample to between 7% and 56% at a 95% binomial confidence interval (see Cameron 2011, for calculation details).

The c_{SB} distributions of X-ray and SZ samples, broken up into low-z and high-z groups, are shown in Figure 4. We perform a

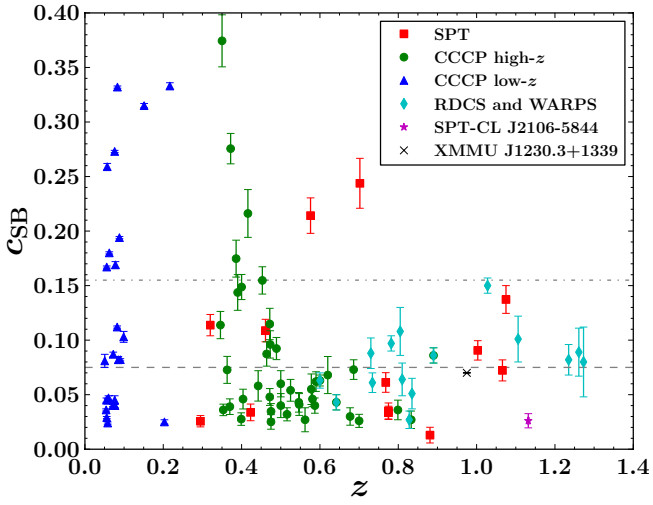

Figure 3. Surface brightness concentration as a function of redshift for objects with a measured c_{SB} included in this study. Four galaxy clusters are members of two surveys and are shown with symbols from both surveys. The dashed line at $c_{SB} = 0.075$ corresponds to the boundary between noncool-core and moderate cool-core clusters. The dash-dotted line at $c_{SB} = 0.155$ corresponds to the boundary between moderate and strong cool-core clusters.

K-S test between the SPT high-z sample and the X-ray high-z sample. The result yields a p-value of 0.42, indicating that although the SPT sample contains the only strong cool-core clusters, the two selection methods show no evidence for being drawn from different parent distributions.

In order to study the evolution of the cool-core fraction we compare the c_{SB} distribution of the SPT high-z sample with that of the X-ray-selected low-z sample (Figure 4).[37] A K-S test between the two data sets results in a p-value of 0.87, providing no evidence that these two distributions are drawn from different parent distributions. Therefore, although there is a smaller fraction of strong cool-core clusters in the high-redshift

[37] We do not study the evolution solely within the SPT sample because at $z < 0.5$, the sample has only four clusters.

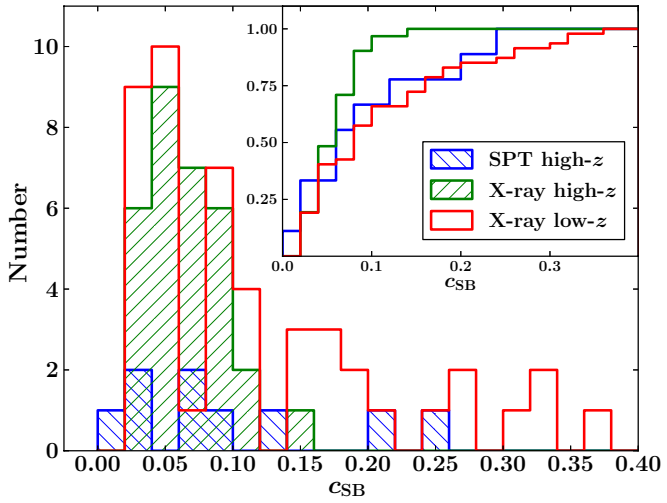

Figure 4. Distribution of the surface brightness concentration of the X-ray high-z sample (the $z \geqslant 0.5$ clusters in the CCCP high-z sample and the $z > 0.6$ clusters in the RDCS+WARPS samples; green forward-hatched areas), the X-ray low-z sample (the $z < 0.5$ clusters from the CCCP high-z sample and the CCCP low-z sample; red empty areas), and the SPT high-z clusters (the $z > 0.5$ clusters from the SPT sample; blue back-hatched areas). Insert: cumulative distribution of the surface brightness concentration for the same three samples.

SPT sample, these results provide no evidence for evolution of the cool-core fraction between the two redshift regimes.

4.4. Investigation of AGN Contamination

Potentially, strong radio emission from AGNs in cool-core clusters could affect their SZ detections. Previous investigations suggest that this should not be a significant concern for samples selected at 150 GHz (Lin et al. 2009; Sehgal et al. 2010). A11 investigate the role radio AGNs play specifically for the SPT sample. Using the Sydney University Molonglo Sky Survey (Mauch et al. 2003) at 843 MHz, A11 identify radio sources in the centers of 7 of the 13 clusters from the SPT sample. They extrapolate the radio flux to the SPT bands and find the total flux of these sources to be negligible compared to the SZ signal.

Measurement of c_{SB} can be affected by the presence of an X-ray-loud AGN within the core radius of the cluster. Such systems result in inflated c_{SB} values due to the AGN's contribution to the core X-ray counts. In this section, we investigate AGN contamination in the moderate and strong cool-core clusters from the SPT sample.

While there are many signatures that a galaxy contains an AGN, there is no definitive diagnostic that the AGN is emitting X-rays besides direct observation of X-rays. Therefore, with the high resolution data provided by *Chandra*, the best way of identifying such features is to visually inspect the images to investigate whether any point sources are within the inner 40 kpc of the cluster center. To validate the visual inspection, we also employ a fully automated source-detection method using the CIAO tool `wavdetect`. We also specifically investigate for the presence of a point source coincident with the X-ray centroid by comparing the hardness ratios of the cluster center with an annulus around the center. The centrally decreasing temperature of a cool-core cluster means that an uncontaminated core will have softer emission in the center than in the annulus. An X-ray AGN, however, has hard X-ray emission and its presence in the cluster core will cause the core to have a higher hardness ratio than the annulus.

Table 4
AGN Signatures for Moderate and Strong Cool-core Clusters

Cluster	HR^{a}_{core}	$HR^{a}_{annulus}$	Central Source	
			Wav[b]	Vis[c]
SPT-CL J0000−5748	$-0.48^{+0.07}_{-0.09}$	$-0.39^{+0.07}_{-0.08}$	Yes	No
SPT-CL J0509−5342	$-0.51^{+0.15}_{-0.15}$	$-0.08^{+0.12}_{-0.12}$	No	No
SPT-CL J2331−5051	$-0.58^{+0.11}_{-0.15}$	$-0.39^{+0.12}_{-0.14}$	No	No
SPT-CL J2341−5119	$-0.64^{+0.16}_{-0.19}$	$-0.35^{+0.12}_{-0.13}$	No	No
SPT-CL J2342−5411	$-0.66^{+0.13}_{-0.19}$	$-0.53^{+0.14}_{-0.18}$	No	No
SPT-CL J2355−5056	$-0.73^{+0.13}_{-0.23}$	$-0.52^{+0.18}_{-0.18}$	No	No

Notes.
[a] Hardness ratio calculated in the cluster core and its surrounding annulus. A core with a lower hardness ratio than its annulus is consistent with no contamination from an X-ray AGN.
[b] Indication of a source detection by `wavdetect` at the cluster center.
[c] Indication of an X-ray point source within the inner 40 kpc of the cluster center based on visual inspection of the observations.

We utilize BEHR (Park et al. 2006), a fully Bayesian approach to calculate hardness ratios that treats photon counts as Poisson statistics with appropriate error propagation. We use an X-ray hardness ratio defined as $(H - S)/(H + S)$ where H corresponds to the X-ray counts in the hard band (2–8 keV) and S is the X-ray counts in the soft band (0.5–2 keV). The hardness ratio of the core is taken in a 2 arcsec aperture centered on the X-ray centroid. This aperture size is used as it would capture approximately 90% of the X-rays from a point source located in its center. The annulus has an inner radius of 2 arcsec and an outer radius of 4 arcsec.

In Table 4, we give the results of our checks for AGN contamination. Visual inspection of the *Chandra* images reveals no evidence of an X-ray point source within 40 kpc of any of the cluster centers. The source-detection tool `wavdetect` only detected a source in the center of one cluster: SPT-CL J0000−5748. In this case, the ratio of the size of the detection with the size of *Chandra*'s point-spread function at the source location is 1.8, indicating the detected source is more extended than a point source (e.g., an AGN) and the emission comes from the cluster's cool-core ICM. In addition, the core hardness ratios range from $-0.73^{+0.13}_{-0.23}$ to $-0.48^{+0.07}_{-0.09}$ and are all lower than the hardness ratios in their surrounding annulus. These core hardness ratios are also softer than the hardness ratios of typical AGNs. For example, Hickox et al. (2009) report a hardness ratio of -0.37 ± 0.06 for a stack of 95 radio-selected AGNs. Therefore, we find no evidence for AGN contamination in our c_{SB} measurements for the SPT sample.

5. DYNAMICAL STATE AND COOL-CORE STRENGTHS

In this section, we examine the relationship between a cluster's dynamical state and its cool-core strength. This can be used to investigate the effect of mergers on the cool-core properties of our sample. For this analysis, we characterize a cluster's dynamical state based on the offset of its BCG from the center of its X-ray emission (Katayama et al. 2003). Having a complete sample is less important here because the BCG position is not involved in our selection techniques. Therefore, in this section, we include SPT-CL J2106−5844 in the SPT sample.

The BCG offsets are determined from the projected distance between the X-ray centroid (as described for the c_{SB} calculation in Section 3.1) and the BCG positions reported in Song et al.

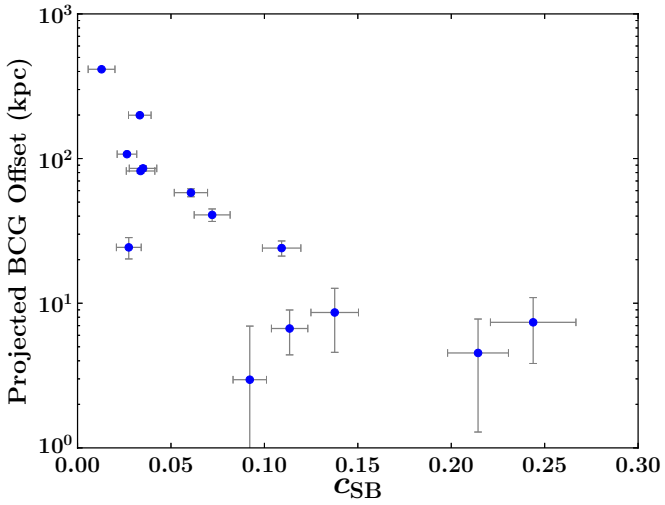

Figure 5. Projected offset between the X-ray centroid and the BCG as a function of c_{SB}. Errors in the BCG offset correspond to the resolution limit of *Chandra* at the cluster's redshift. Data from the SPT sample and SPT-CL J2106−5844.

(A color version of this figure is available in the online journal.)

(2012). Uncertainties in the offsets are given as the resolution for the *Chandra* observations at each cluster's redshift.

Although the majority of local clusters exhibit relatively small BCG offsets (Lin & Mohr 2004), Sanderson et al. (2009) show that the magnitude of this offset is anticorrelated with the cool-core strength of the cluster. As shown in Figure 5, the offsets for our SZ-selected sample are in agreement with these results. We find a strong anticorrelation between c_{SB} and the BCG offset as well as an absence of noncool cores with low offsets. The two parameters exhibit a Spearman's rank correlation coefficient of $\rho = -0.83$ with a p-value of 2.2×10^{-4}. These results reinforce the model that as clusters relax, BCGs settle in the center of the potential well and cool cores become established. Later, dynamical disturbances are capable of removing a cool core. Within this model, the clean anticorrelation reinforces c_{SB} as a parameter that accurately measures cluster cores at high redshifts. The lack of "relaxed," noncool-core clusters with small BCG offsets suggests that neither preheating (as proposed by Kaiser 1991; McCarthy et al. 2008) nor strong AGN feedback (as reviewed in Fabian 2012; McNamara & Nulsen 2012) are the most dominant mechanisms of cool-core disruption in our sample. Rather, this anticorrelation points to recent mergers playing a major role by mixing or shock-heating the ICM.

6. CONCLUSIONS

We study the cool-core characteristics of an SZ-selected cluster sample detected by the SPT survey. The sample provides an alternative to the existing X-ray-selected samples for studying the cool-core fraction at high redshifts, which may be impacted by X-ray selection effects.

We evaluate the two parameters that are suitable for measuring cool cores at high redshifts, the concentration of surface brightness (c_{SB}) and the cuspiness (α), and examine their performance as a predictor of the central cooling time t_{cool}. A Spearman's rank test shows correlation coefficients between α and t_{cool} and between c_{SB} and t_{cool} to be $\rho_\alpha = -0.88$ and $\rho_{c_{SB}} = -0.84$, respectively. However, c_{SB} exhibits much smaller fractional measurement errors.

Using c_{SB}, we find evidence of two strong cool-core clusters in the SPT sample at $z > 0.5$, among the first of their kind. We rule out the hypothesis that there are no such galaxy clusters at the 5.4σ level. With a sample of nine high-redshift clusters, we show that the high-z strong cool-core fraction is greater than 7% with 95% confidence. We compare the distributions of the SPT sample and previous X-ray-selected samples with a K-S test. The result yields a p-value of 0.42, providing no statistically significant evidence that the two samples are drawn from different distributions.

We also evaluate the relationship between the strength of a cluster's cool core and its dynamical state. We find a strong anticorrelation between c_{SB} and the offset between the BCG and the X-ray centroid, which is related to the dynamical state of the cluster. While preheating or AGN feedback may be responsible for the lack of cool cores in some clusters, this result suggests that in our sample, the formation of cool cores is inhibited by merger events in clusters, which cause turbulent mixing or shock-heating of the ICM.

The results of this study are based on a complete sample of SZ-selected clusters with *Chandra* observations sampled from the first 178 deg^2 of the SPT survey. The statistics of our results will soon be dramatically improved through a *Chandra* X-ray Visionary Project underway to observe the 80 most significant clusters at $z > 0.4$ from the first 2000 deg^2 of the SPT survey.

The South Pole Telescope program is supported by the National Science Foundation through grant ANT-0638937. The Munich group is supported by The Cluster of Excellence "Origin and Structure of the Universe," funded by the Excellence Initiative of the Federal Government of Germany, EXC project No. 153. Galaxy cluster research at the University of Chicago is partially supported by Chandra award No. GO2-13006A issued by the Chandra X-ray Observatory Center. Partial support is also provided by the NSF Physics Frontier Center grant PHY-0114422 to the Kavli Institute of Cosmological Physics at the University of Chicago, the Kavli Foundation, and the Gordon and Betty Moore Foundation. Galaxy cluster research at Harvard is supported by NSF grant AST-1009012. Galaxy cluster research at SAO is supported in part by NSF grants AST-1009649 and MRI-0723073. The McGill group acknowledges funding from the National Sciences and Engineering Research Council of Canada, Canada Research Chairs program, and the Canadian Institute for Advanced Research. X-ray research at the CfA is supported through NASA contract NAS 8-03060. Support for X-ray analysis is provided by the National Aeronautics and Space Administration through Chandra award No. GO0-1114 issued by the Chandra X-ray Observatory Center, which is operated by the Smithsonian Astrophysical Observatory for and on behalf of the National Aeronautics Space Administration under contract NAS8-03060. R.J.F. is supported by a Clay Fellowship. B.A.B is supported by a KICP Fellowship. M. Bautz and M.M acknowledge support from contract 2834-MIT-SAO-4018 from the Pennsylvania State University to the Massachusetts Institute of Technology. M.M acknowledges support from NASA Hubble fellowship grant HST-HF-51308.01. M.D. acknowledges support from an Alfred P. Sloan Research Fellowship, C.J. acknowledges support from the Smithsonian Institution, and B.S. acknowledges support from the Brinson Foundation. The authors thank Marcella Brusa for her helpful discussion.

REFERENCES

Andersson, K., Benson, B. A., Ade, P. A. R., et al. 2011, ApJ, 738, 48
Benson, B. A., de Haan, T., Dudley, J. P., et al. 2011, ApJ, submitted (arXiv:1112.5435)

Burenin, R. A., Vikhlinin, A., Hornstrup, A., et al. 2007, ApJS, 172, 561
Cameron, E. 2011, PASA, 28, 128
Eckert, D., Molendi, S., & Paltani, S. 2011, A&A, 526, A79
Edge, A. C., Stewart, G. C., Fabian, A. C., & Arnaud, K. A. 1990, MNRAS, 245, 559
Fabian, A. C. 2012, ARA&A, 50, 455
Fabian, A. C., & Nulsen, P. E. J. 1977, MNRAS, 180, 479
Fassbender, R., Böhringer, H., Santos, J. S., et al. 2011, A&A, 527, A78
Foley, R. J., Andersson, K., Bazin, G., et al. 2011, ApJ, 731, 86
Gómez, P. L., Loken, C., Roettiger, K., & Burns, J. O. 2002, ApJ, 569, 122
Gottlöber, S., Klypin, A., & Kravtsov, A. V. 2001, ApJ, 546, 223
Hickox, R. C., Jones, C., Forman, W. R., et al. 2009, ApJ, 696, 891
Horner, D. J., Perlman, E. S., Ebeling, H., et al. 2008, ApJS, 176, 374
Hudson, D. S., Mittal, R., Reiprich, T. H., et al. 2010, A&A, 513, A37
Jeltema, T. E., Hallman, E. J., Burns, J. O., & Motl, P. M. 2008, ApJ, 681, 167
Kaastra, J. S., Ferrigno, C., Tamura, T., et al. 2001, A&A, 365, L99
Kaiser, N. 1991, ApJ, 383, 104
Katayama, H., Hayashida, K., Takahara, F., & Fujita, Y. 2003, ApJ, 585, 687
Komatsu, E., Smith, K. M., Dunkley, J., et al. 2011, ApJS, 192, 18
Lin, Y., Partridge, B., Pober, J. C., et al. 2009, ApJ, 694, 992
Lin, Y.-T., & Mohr, J. J. 2004, ApJ, 617, 879
Mathews, W. G., & Bregman, J. N. 1978, ApJ, 224, 308
Mauch, T., Murphy, T., Buttery, H. J., et al. 2003, MNRAS, 342, 1117
McCarthy, I. G., Babul, A., Bower, R. G., & Balogh, M. L. 2008, MNRAS, 386, 1309
McDonald, M. 2011, ApJ, 742, L35
McDonald, M., Bayliss, M., Benson, B. A., et al. 2012, Nature, 488, 349
McDonald, M., Veilleux, S., & Mushotzky, R. 2011, ApJ, 731, 33
McGlynn, T. A., & Fabian, A. C. 1984, MNRAS, 208, 709
McNamara, B. R., & Nulsen, P. E. J. 2012, New J. Phys., 14, 055023
Molendi, S., & Pizzolato, F. 2001, ApJ, 560, 194
Motl, P. M., Hallman, E. J., Burns, J. O., & Norman, M. L. 2005, ApJ, 623, L63
Nagai, D. 2006, ApJ, 650, 538
O'Hara, T. B., Mohr, J. J., Bialek, J. J., & Evrard, A. E. 2006, ApJ, 639, 64
Park, T., Kashyap, V. L., Siemiginowska, A., et al. 2006, ApJ, 652, 610
Parrish, I. J., McCourt, M., Quataert, E., & Sharma, P. 2012, MNRAS, 422, 704
Peterson, J. R., Paerels, F. B. S., Kaastra, J. S., et al. 2001, A&A, 365, L104
Reichardt, C. L., Stalder, B., Bleem, L. E., et al. 2012, ApJ, submitted (arXiv:1203.5775)
Rosati, P., della Ceca, R., Norman, C., & Giacconi, R. 1998, ApJ, 492, L21
Russell, H. R., Fabian, A. C., Taylor, G. B., et al. 2012, MNRAS, 422, 590
Samuele, R., McNamara, B. R., Vikhlinin, A., & Mullis, C. R. 2011, ApJ, 731, 31
Sanderson, A. J. R., Edge, A. C., & Smith, G. P. 2009, MNRAS, 398, 1698
Santos, J. S., Rosati, P., Tozzi, P., et al. 2008, A&A, 483, 35
Santos, J. S., Tozzi, P., Rosati, P., & Böhringer, H. 2010, A&A, 521, A64
Santos, J. S., Tozzi, P., Rosati, P., Nonino, M., & Giovannini, G. 2012, A&A, 539, A105
Sehgal, N., Bode, P., Das, S., et al. 2010, ApJ, 709, 920
Siemiginowska, A., Burke, D. J., Aldcroft, T. L., et al. 2010, ApJ, 722, 102
Song, J., Zenteno, A., Stalder, B., et al. 2012, ApJ, 761, 22
Sun, M. 2009, ApJ, 704, 1586
Sunyaev, R. A., & Zel'dovich, Y. B. 1972, Comments Astrophys. Space Phys., 4, 173
Tamura, T., Bleeker, J. A. M., Kaastra, J. S., Ferrigno, C., & Molendi, S. 2001, A&A, 379, 107
Vanderlinde, K., Crawford, T. M., de Haan, T., et al. 2010, ApJ, 722, 1180
Vikhlinin, A., Burenin, R., Forman, W. R., et al. 2007, in Heating versus Cooling in Galaxies and Clusters of Galaxies, ed. H. Böhringer, G. W. Pratt, A. Finoguenov, & P. Schuecker (Berlin: Springer), 48
Vikhlinin, A., Burenin, R. A., Ebeling, H., et al. 2009, ApJ, 692, 1033
ZuHone, J. A., Markevitch, M., & Johnson, R. E. 2010, ApJ, 717, 908